



# Defective eyelid leading edge cell migration in C57BL/6-corneal opacity mice with an “eye open at birth” phenotype

L.C. Wu<sup>1</sup>, C. Liu<sup>2</sup>, M.R. Jiang<sup>1</sup>, Y.M. Jiang<sup>1</sup>, Q.H. Wang<sup>1</sup>, Z.Y. Lu<sup>1</sup>,  
S.J. Wang<sup>1</sup>, W.L. Yang<sup>1</sup> and Y.X. Shao<sup>1,2</sup>

<sup>1</sup>Laboratory Animals Center, Nantong University, Nantong, China

<sup>2</sup>Institute of Comparative Medicine, Nantong University, Nantong, China

Corresponding author: Y.X. Shao

E-mail: shaoyx@ntu.edu.cn

Genet. Mol. Res. 15 (3): gmr.15036741

Received May 7, 2015

Accepted May 25, 2016

Published August 26, 2016

DOI <http://dx.doi.org/10.4238/gmr.15036741>

Copyright © 2016 The Authors. This is an open-access article distributed under the terms of the Creative Commons Attribution ShareAlike (CC BY-SA) 4.0 License.

**ABSTRACT.** Development of the eyelid requires coordination of the cellular processes involved in proliferation, cell size alteration, migration, and cell death. C57BL/6J-corneal opacity (B6-Co) mice are mutant mice generated by the administration of N-ethyl-N-nitrosourea (100 mg/kg). They exhibit the eyelids open at birth phenotype, abnormal round cell shape from tightened F-actin bundles in leading edge keratinocytes at E16.5, and gradual corneal opacity with neovessels. The tip of the leading edge in B6-Co mice did not move forward, and demonstrated a sharp peak shape without obvious directionality. Analysis of the biological characteristics of B6-Co mice demonstrated that abnormal migration of keratinocytes could affect eyelid development, but proliferation and apoptosis in B6-Co mice had no effect. Mutant gene mapping and sequence analysis demonstrated that in B6-Co mice, adenosine was inserted into the untranslated regions,

between 3030 and 3031, in the mRNA 3'-terminal of Fgf10. In addition, guanine 7112 was substituted by adenine in the Mtap1B mRNA, and an A2333T mutation was identified in Mtap1B. Quantitative real-time polymerase chain reaction analysis showed that expression of the Hbegf gene was significantly down-regulated in the eyelids of B6-Co mice at E16.5, compared to B6 mice. However, the expression of Rock1, Map3k1, and Jnk1 genes did not show any significant changes. Abnormal keratinocyte migration and down-regulated expression of the Hbegf gene might be associated with impaired eyelid development in B6-Co mice.

**Key words:** B6-Co mouse; Leading edge; Keratinocyte migration; Eyelid development; Gene expression

## INTRODUCTION

During normal development in mammals, the eyelids grow across the eye, fuse, and subsequently reopen. In mice, the periderm forms an outer layer of the epidermis on days 10 and 11 of gestation (E10 and E11). It is one-cell thick and covers the outer surface of the embryo from day E12 until it is shed on day E17. During this period the underlying epidermis rapidly proliferates and differentiates to become a stratified, keratinized epithelium. The upper and lower eyelids are fused to each other on day E16.5 and reopen on about postnatal day (P) 14 (Harris and Juriloff, 1986). The gaping lids (gp) or lidgap-Gates (lgGa) mutations, which cause the eyelids open at birth phenotype in mice, were discovered in 1961. They exhibit autosomal recessive inheritance spontaneously developed from C57BL/6-ax stain mice with 100% penetrance (Ricardo and Miller, 1967). The mutant gene was mapped to a chromosome between D13Mit76 (62.35 cM) and D13Mit53 (63.73 cM) using microsatellite genetic markers. There is a 27.5-kb deletion including exons 2-9 in the Map3k1 gene of lgGa mice (Juriloff et al., 2005).

Mice with eyelids open at birth are generally referred to as having an eye open at birth (EOB) phenotype. EOB mice gradually develop corneal disease, which mainly presents as keratitis and corneal opacity. The developmental process of this phenotype mimics relevant diseases in humans. Therefore, the EOB mouse model is very useful for characterization of the molecular mechanisms underlying the process of eyelid closure and fusion.

In our previous study, heredity C57BL/6J-corneal opacity (B6-Co) mice were generated by administering N-ethyl-N-nitrosourea (ENU) (100 mg/kg) to wild-type C57BL/6 mice (Shao et al., 2006). The eyes of these mice were open at birth, and the cornea gradually became opaque. The mutant gene was located between 112,546,283 and 113,397,654 bp on chromosome 13, determined by single nucleotide polymorphism (SNP) fine mapping (Jiang et al., 2010). In the present study, histochemical analysis was conducted to phenotypically characterize B6-Co mice at different embryonic stages. The wound healing assay, 5-bromo-2-deoxyuridine (BrdU) staining, and TUNEL assay were used to investigate migration, proliferation, and apoptosis, respectively, of keratinocytes in the eyelids of B6-Co mice. Reverse transcription-polymerase chain reaction (RT-PCR) was used to test the expression of genes involved in eyelid development. B6-Co mice are an excellent model for investigating the mechanisms of eyelid development, and exploring drug targets for treating human cornea matrix denaturalization.

## MATERIAL AND METHODS

### Laboratory animals

B6-Co, a mutant mouse model on a C57BL/6J (B6) background, and wild-type B6 mice were both obtained from the Laboratory Animal Center of Nantong University. Mice were kept in a barrier system at  $23^{\circ} \pm 2^{\circ}\text{C}$  with humidity of  $55 \pm 5\%$ . The mice were maintained under a 12-h light/12-h dark cycle with free access to radiation-sterilized food (Shuangshi, Suzhou, China) and sterile water.

All experimental procedures involving animals were conducted in accordance with the Institutional Animal Care guidelines, and were ethically approved by the administration committee of experimental animals, Jiangsu Province, China.

### Phenotypic characterization

The corneal opacity of B6-Co mice was examined under a slit lamp. Fetuses of E14.5-P0 were sacrificed by decapitation, and heads were collected for phenotypic characterization. The heads of fetuses were fixed in 4% paraformaldehyde overnight at  $4^{\circ}\text{C}$ , dehydrated with a graded sucrose solution series, and embedded in Tissue Freezing Medium (O.C.T). Tissues were then cut into 8- $\mu\text{m}$  thick frozen sections using a freezing microtome of Leica CM1900 (Leica, Solms, Germany). The sections were then subjected to hematoxylin and eosin (H&E) staining before acquiring images using a color digital camera. The tissue sections were incubated with FITC-phalloidin and Hoechst 33342 (Sigma, San Jose, CA, USA) and observed under a fluorescence microscope of Olympus cxx41 (Olympus, Tokyo, Japan).

### Cell culture

Primary mouse epidermal keratinocytes and dermal fibroblasts were prepared from B6 and B6-Co E16.5 fetuses. B6-Co pups displayed the EOB phenotype. Keratinocytes were prepared as previously described (Zhang et al., 2003b) and all cell culture reagents were obtained from Hyclone (Hyclone, Logan, UT, USA).

### *In vitro* wound-healing assay

Confluent monolayers of B6 and B6-Co epidermal keratinocytes and dermal fibroblasts were starved in growth factor-free media for 24 h before being wounded by scratching the monolayer with a micropipette tip. The wounded cells were then washed, and cultured at  $37^{\circ}\text{C}$  in the appropriate media with or without growth factors. Images of the wounded area were acquired 24 h after wounding.

### BrdU incorporation

The proliferation of keratinocytes was determined using a BrdU labeling/detection kit (Sigma), according to the manufacturer instructions. After BrdU labeling, the keratinocytes were observed under a fluorescent microscope. The percentage of BrdU-positive cells was calculated from 10 random fields in 3 wells.

## ***In vitro* apoptosis assay**

Keratinocytes isolated from the eyelids of E16.5 mice were used to detect apoptotic cells. A TUNEL assay was performed on samples using the One Step TUNEL Apoptosis Assay Kit, according to the manufacturer instructions (Beyotime, Haimen, China).

## **Sequence analysis and real-time PCR**

Total RNA was isolated from B6-Co and B6 embryos using the TRIzol kit, according to the manufacturer instructions (Invitrogen, Carlsbad, CA, USA). Full-length cDNA was synthesized using RevertAid™ M-MuLV reverse transcriptase (Fermentas, Burlington, Canada) and was then amplified by PCR using Taq polymerase (Fermentas, Burlington, Canada). The primers were designed using the Primer Prepmer 5.0 software (Premier, Toronto, Canada) (Table 1). The RT-PCR products for Fgf10, and Mtap1B were 1138 and 938 bp, respectively.

PCR products were gel purified using the EZ Spin Column DNA Gel Extraction Kit (Sangon, Shanghai, China), and recombinant vectors were transformed in competent cells after DNA fragments were cloned into the pGEM-T vector (Promega, Madison, WI, USA). Positive clones were identified by *Eco*RI restriction endonuclease digestion and sequence analysis (Sangon).

Total RNA were extracted from eyelid tissues in B6-Co and B6 embryos for real-time PCR using Fast EvaGreen® qPCR Master Mix (Biotium, Hayward, CA, USA). The primers were designed using the Primer Prepmer 5.0 software (Table 1). The PCR products for Gapdh, Hbegf, Rock1, Map3k1, and Jnk1 were 133, 182, 117, 172, and 162 bp, respectively. The reactions were cycled 45 times under the appropriate parameters for each pair of primers and the fluorescence was measured every 15 s at the end of each cycle to construct the amplification curve. All determinations were performed at least in triplicate. The relative expression of mRNAs was calculated using the comparative  $2^{-\Delta\Delta C_t}$  method and normalized against Gapdh.

**Table 1.** Oligonucleotide primers used for RT-PCR.

Targets	Gene locus	Sequence (5' to 3')	Length (bp)
Fgf10	NM_008002	F: AAGGTATAGAAAGCAGTATGTAAG R: TCCCACGGAGGCAGAA	1138
Mtap1B	NM_008634	F: TGATGGGAAAGTCCAAGCC R: AAATGCCAATACCTAGCAGAAG	938
Gapdh	NM_008084	F: GGAGCGAGACCCCACTAAC R: GGCGGAGATGATGACCCT	136
Hbegf	NM_010415	F: GCCTCAGGAAATACAAGGACTA R: TACAGCCACCACAGCCAAG	182
Rock1	NM_009071	F: CAGATGAAACTGATGGAAACCT R: TGCTGCTTACCACAACATACTG	117
Map3k1	NM_011945	F: GGTCTAAGAGGTCAGCAGTATG R: GGACAGGTGTGACGGGATG	178
Jnk1	NM_016700	F: AGAGGGAGCACACAATAGAGG R: ACAGACGGCGAAGACGAT	162

## **Statistical analysis**

All data are reported as means  $\pm$  SE of three independent experiments (each in duplicate). One-way ANOVA and the *post hoc* Scheffe test were used for statistical analysis using the Stata 6.0 software package (Stata, College Station, TX, USA). P values <0.05 were considered to be statistically significant.

## RESULTS

### Eyelid closure defect at birth in B6-Co mice

B6 mice were crossed with B6-Co mice to generate normal wild-type and B6-Co phenotype mice. To define the pathological structure of the eyelid defect in B6-Co mice, we initially analyzed the histology of eyelid formation and development. The phenotype of embryonic eyelids in B6-Co mice was extremely similar to that in B6 mice at E14.5 (Figure 1A I-III and B I-III). However, at E16.5, the ocular surface in B6 mice was covered by a thin epithelium that extended from the tip of the developing eyelid, described as membrane-like eyelids (Figure 1C I-III). In contrast, the eyelids of B6-Co grew more slowly than that of B6 (Figure 1D I), leaving the ocular surface exposed (Figure 1D II and D III), and this corresponded with the development process (Figure 1E I-III and F I-III). The eyelids opened in B6-Co mice at P0 (Figure 1H I-III), but were fused tightly in B6 mice at the same time point (Figure 1G I-III).

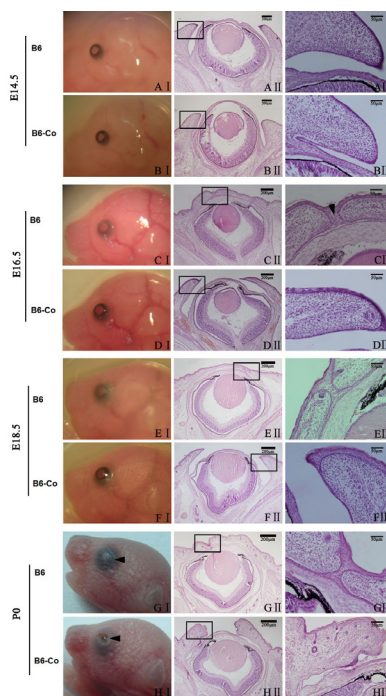


**Figure 1.** Morphological observation of eyelids in B6 and B6-Co mice at different embryonic stages. **I.** Image of the eyelid obtained from a stereomicroscope. **II.** and **III.** H&E staining of the embryonic eyelids. **A.** and **B.** E14.5: the eyelids have just started to grow, and the eyelid phenotypes are not different from the fetus at the embryo stage. **C.** and **D.** E16.5: Eyelid closure is complete in normal mice, and the cells are loose (arrowhead) at the fusion line of the upper and lower eyelids. The forward migration of upper and lower eyelids in B6-Co mice was blocked and the eyelids were not fused, demonstrating defects in eyelid development. **E.** and **F.** E18.5: the eyelids continue to grow and develop in normal mice, and accessory structures such as the hair follicle are shown. The eyelids stopped developing in B6-Co mice, and the defect in the pathology of the eyelids is more evident at this stage. **G.** and **H.** P0: the cells are loose at the fusion line of the upper and lower eyelids, but the eyelids are tightly closed (arrowhead) in normal mice. B6-Co mice demonstrate the eye open phenotype and short eyelids, and there were hair follicles in the eyelids of normal and B6-Co mice.

## Eyelids open at birth and the cornea gradually becomes opaque in B6-Co mice

The eyelids are tightly closed at birth (Figure 2AI) and reopen approximately at P14 in B6 mice. Furthermore, cornea development was normal in B6 mice (Figure 2AII and AIII). However, the eyelids opened at birth (Figure 2BI) in B6-Co mice, leaving the cornea exposed, leading to gradual opacity (Figure 2BII and BIII) and neovessel formation (Figure 2BIII, arrowhead). Previous studies indicate that the EOB phenotype completely correlates with corneal opacity in B6-Co mice (Jiang et al., 2010). B6-Co mice with abnormal eyelid development suffer from infection of the cornea, and its epithelium is destroyed by P3. Corneal opacity gradually develops by P10, when neovessels appear, as described in our previous study (Tang et al., 2008).

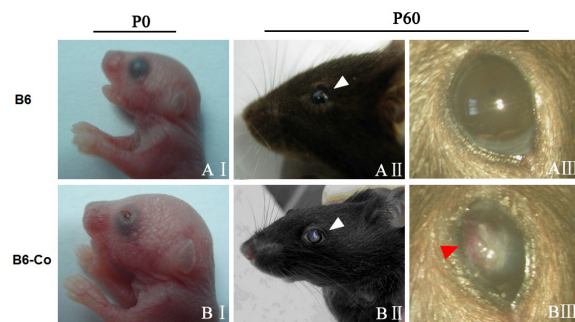


**Figure 2.** Eyelids opened at birth and gradual corneal opacity in B6-Co mice. **I.** P0 mice. **II.** and **III.** P60 mice. Observation of eye phenotype was performed using a slit lamp (III). **A.** B6 mice with closed eyelids at birth, and transparent cornea at p60 (arrowhead). **B.** B6-Co mutant mice with open eyelids at birth, and corneal opacity with neovessels (red arrowhead).

## Defects in F-actin development in leading edge cells of B6-Co mice

Development of the eyelid requires coordination of the cellular processes of proliferation, cell morphology, migration, and cell death. Cell migration was related to morphous changes of actin filaments, which significantly affect the cytoskeleton (Lin et al., 2015). We detected morphous F-actin filaments in the eyelids of mice at different embryonic stages using FITC-phalloidin staining. At E16.5, the shape of the cytoskeleton of leading edge cells was similar to the ellipse or spindle shape observed in B6 eyelids (Figure 3AI, arrowheads). F-actin bundles were assembled, recombination and extension continually, which elongated the cells (Figure 3AII and AIII). The continuous forward movement of upper and lower eyelids was based on cell proliferation and continual extension. In contrast, there were very few F-actin bundles assembled in the leading edge cells, and the cells exhibited a round pie shape with tightly arranged F-actin bundles in B6-Co mice (Figure 3BI-III). The tip of the leading edge (Figure 3AII, red arrowhead) had a sharp peak shape that allowed forward movement in B6 mice. In contrast, a blunt terminal was observed in B6-Co mice (Figure 3BII), with no obvious directional movement. The leading edge hardly moved forward, although the embryo continued to develop (Figure 3CI-III and EI-III). There was no significant difference in the shape of microfilament bundles in leading edge cells in B6 and B6-Co mice at E18.5 (Figure 3CI-III and DI-III) and P0 (Figure 3EI-III and FI-III). The morphology of the nucleus

in leading edge cells differed from that of cells at other positions in eyelids (Figure 3II, dotted lines). The number of keratinocyte nuclei in the eyelids of B6-Co mice was not significantly different from that of B6.

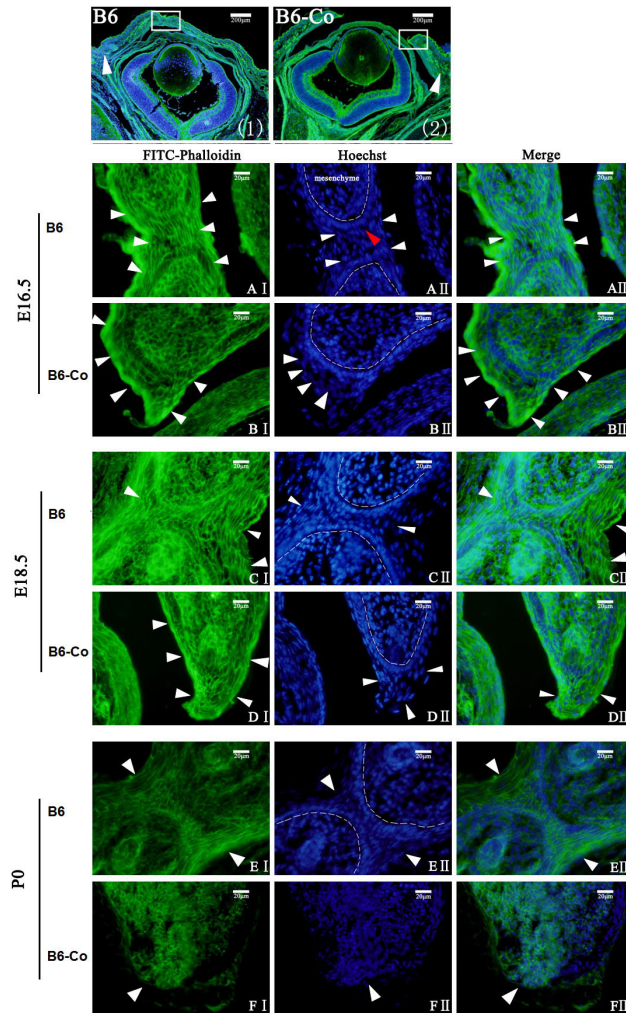


**Figure 3.** FITC-phalloidin and Hoechst staining of eyelid position in B6 and B6-Co mice at different embryonic stages. **1.** and **2.** Contour maps of eyelid position by FITC-phalloidin and Hoechst staining in B6 and B6-Co mice at E16.5. Arrowheads represent the root region. **I.** FITC-phalloidin staining. **II.** Hoechst staining. **III.** Merged image of both stains. **A.** and **B.** E16.5: the cell morphology was different between B6 and B6-Co mice (arrowheads), and the cytoskeletal morphological difference was significant between AI and BI, and there were F-actin bundles assembled in a similar ellipsoidal shape in the AI cells in the stretch state but not in the same state in BI. A series of cells compose the leading edge near the dotted line. The red arrowhead shows the tip of the leading edge in AII, and the inner dotted line represents mesenchyme. **C.** and **D.** E18.5: the leading edges of the upper and lower eyelids were closer in CII, and the cytoskeleton morphology between CI and DI was not significantly different from AI and BI. **E.** and **F.** P0: the upper and lower eyelids remain closed in EI, and the cytoskeleton morphology was not significantly different from FI. The leading edge was not obvious in FII. The light degree of Hoechst staining and the nuclear density were not significantly different between B6 and B6-Co from II.

### Proliferation and migration of keratinocytes isolated from B6-Co mice

To investigate the mechanisms underlying the defects in eyelid development in B6-Co mice, BrdU incorporation and wound healing assays were used to assess the proliferation and migration of keratinocytes isolated from the eyelids of B6-Co mice. The *in vitro* BrdU incorporation assay demonstrated no significant difference ( $P = 0.069$ ) in keratinocyte proliferation between B6 and B6-Co mice at E16.5 (Figure 4). However, keratinocyte migration was decreased in B6-Co mice compared to B6 mice ( $P = 0.012$ ), which was detected 24 h after scratching in an *in vitro* wound healing assay (Figure 5). Furthermore, B6 and B6-Co keratinocytes at E16.5 were subjected to a TUNEL assay to examine apoptosis around the eyelid tissues. However, no significant difference ( $P = 0.371$ ) in apoptosis was observed between the keratinocytes isolated from B6-Co and B6-Co mice at E16.5 (Figure 6).

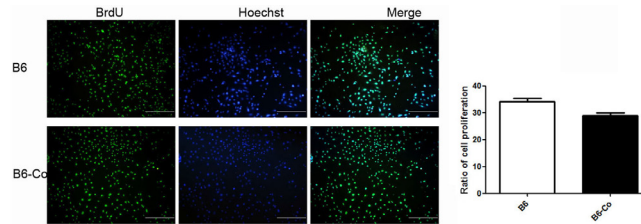


**Figure 4.** Keratinocyte proliferation in eyelids in B6 and B6-Co mice. Representative BrdU incorporation image for keratinocytes in B6 and B6-Co mice. Error bars represent means  $\pm$  SD from three independent experiments. Scale bar: 200  $\mu$ m.

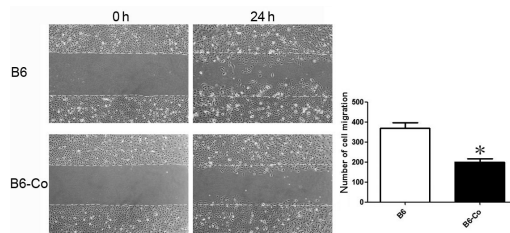


**Figure 5.** Keratinocyte migration in B6 and B6-Co mice using an *in vitro* wound healing assay. Confluent monolayers of B6 and B6-Co mice epidermal keratinocytes were subjected to *in vitro* wound-healing assays in medium without growth factors. Images were acquired 24 h after wounding. Error bars represent means  $\pm$  SD from three independent experiments. \* $P = 0.012$  versus B6.

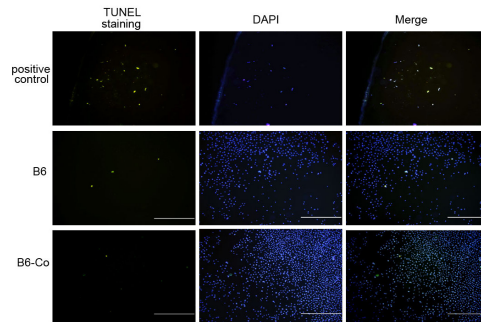


**Figure 6.** TUNEL staining. Keratinocytes of B6 and B6-Co mice at E16.5 were subjected to a TUNEL assay to examine apoptosis around the eyelid tissues. Positive controls were eyelid tissues treated with DNase I. Scale bar: 200  $\mu$ m.

## Mutant gene mapping and candidate gene analysis

We previously showed that the mutant gene causing the EOB phenotype was roughly mapped to chromosome 13 (Shao et al., 2006), and further mapped between two SNPs, rs29492976 and rs29620530 (112,546,283 and 113,397,654 bp), by SNPs rs29235242, rs29492976, rs29620530, rs29778277, and rs13466915 (Jiang et al., 2010). There were two candidate genes, *Map3k1* and *Il6st*, in the mapping range, and the *Map3k1* gene was shown to be the candidate gene responsible for the EOB phenotype by *Map3k1* knockout studies (Meng et al., 2014). *Il6st* knockout mice exhibited a blind phenotype induced by retinopathy (Chucair-Elliott et al., 2012). However, B6-Co mice exhibit dominant heredity. Specifically, a single copy mutant gene was sufficient to display the EOB phenotype in B6-Co mice. In contrast homozygous *MEKK1<sup>AKD/AKD</sup>* was required for the EOB phenotype in *Map3k1* knockout mice (Meng et al., 2014).

A sequence analysis for *Map3k1* and *Il6st* genes in B6-Co mice showed no mutations. However, *Fgf10* (67.14 cM) and *Plk2* (61.9 cM) genes, which are associated with eyelid development, were found near the mapping region. The *Mtap1B* (52.9 cM) gene regulates microtubular recombination. Furthermore, *Mtap1B* knockout mice developed blindness due to retinopathy (Meixner et al., 2000; Ma et al., 2003; Tsau et al., 2011). RT-PCR and sequencing analysis were used to confirm mutations in *Fgf10* (Figure 7A and B), *Plk2* (data not shown), and *Mtap1B* (Figure 7F and G) genes, all of which are involved in eyelid development in B6-Co mice. The results of sequencing showed that there was an insertion mutation in the 3'-untranslated region (UTR) of the *Fgf10* gene (Figure 7E). Sequencing of the RT-PCR product of *Mtap1B* (Figure 7F) demonstrated an A2333T mutation in the coding region of the *Mtap1B* gene (Figure 7G) in B6-Co mice (Figure 7H, arrowhead). However, no mutations were identified in the *Plk2* gene of B6-Co mice (data not shown). To confirm the mutations identified in *Fgf10* and *Mtap1B* genes of B6-Co mice, we analyzed ten B6-Co samples, and determined that the mutation rate was 80% in the *Mtap1B* gene and 70% in *Fgf10* (Table 2).

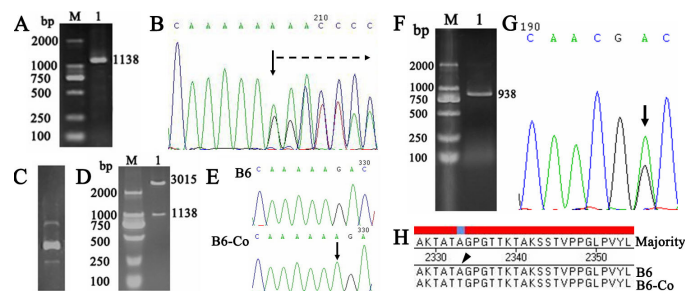


**Figure 7.** RT-PCR, TA cloning, enzyme digestion, and sequencing analysis of partial sequence of *Fgf10* and *Mtap1B* genes. **A.** Electrophoresis of the RT-PCR product of the *Fgf10* gene. Lane M: DL2000 DNA marker. **B.** Analysis of the partial sequence of the *Fgf10* gene. **C.** Electrophoresis of the recombinant plasmid of *Fgf10* in a T-vector. **D.** Electrophoresis of the product of enzyme digestion of the recombinant plasmid of *Fgf10* in a T-vector by *EcoRI*. Lane M: DL2000 DNA marker. **E.** Sequence analysis of cloned *Fgf10* in B6 and B6-Co mice. Arrow was base A inserted between the 3030 and 3031 UTR in the mRNA 3'-terminal of *Fgf10* in B6-Co mice. **F.** Electrophoresis of the RT-PCR product of the *Mtap1B* gene. Lane M: DL2000 DNA marker. **G.** Analysis of the partial sequence of the *Mtap1B* gene. Arrow shows that 7112 base G was substituted by base A in the mRNA of *Mtap1B*. **H.** Amino acid sequence of *Mtap1B* in B6-Co mice compared with B6 mice. Arrowhead shows that Ala<sup>233</sup> was replaced by Thr in *Mtap1B* of B6-Co mice.

**Table 2.** Analysis of Mtap1B and Fgf10 gene mutation in 10 samples.

Gene name	Location (cM)	Mutation in 10 samples ("+" normal, "-" mutant)	Protein coding change
Mtap1B	52.9	- - + - - + - - -	yes
Fgf10	67.14	- + - - - + + - -	no

It was reported that down-regulation of Hbegf and Mtap1B mutation was involved in eyelid development defects in B6-Co mice (Hayashi et al., 2005; Pacal and Bremner, 2014). Hbegf, Rock1, Map3k1, and Jnk1 genes are key factors for eyelid development. To understand the molecular mechanisms underlying the process of eyelid development, we checked the expressions of these genes in the eyelids of B6-Co mice at different embryo stages by real-time PCR. Compared to B6 mice, expression of the Hbegf gene was significantly down-regulated ( $P = 0.043$ ) in B6-Co at E16.5 (Figure 8). However, no significant changes in the expression of Rock1, Map3k1, and Jnk1 genes were observed between B6 and B6-Co mice ( $P > 0.05$ ; Figure 8).

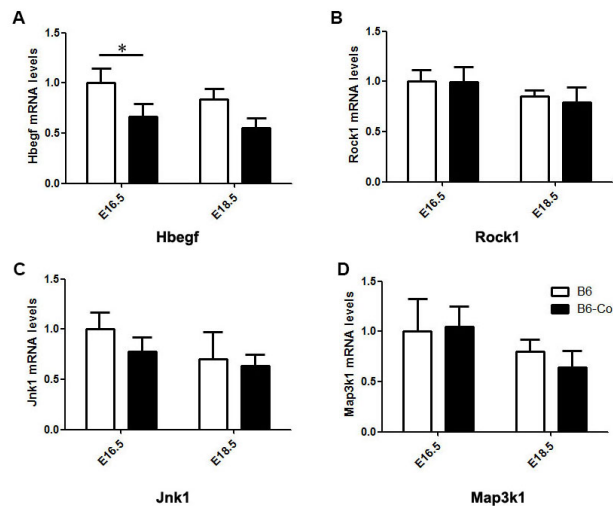


**Figure 8.** RT-PCR detection of relevant genes involved in eyelid development. The expression of Hbegf (A), Rock1 (B), Map3k1 (C), and Jnk1 (D) in the eyelids of B6-Co mice at different embryonic stages was analyzed by real-time PCR. Gapdh was used as an internal control, and each reaction was analyzed in triplicate. \* $P = 0.0431$  versus B6.

## DISCUSSION

B6-Co mice exhibit a relatively normal appearance at birth, except for the fact that they have open eyelids at this primordial stage (Figure 1C and D), and that their corneas gradually become opaque (Figure 2B). The phenotype of B6-Co mice was similar to various gene knockout mice, including *Egfr*, *Tgf $\alpha$* , *Fgfr2*, *Map3k1*, *Hbegf*, *c-jun*, *Lgr4*, and *Rock1* knockouts (Li et al., 2003; Mine et al., 2005; Thumkeo et al., 2005; Kato et al., 2007; Pennock et al., 2011; Martínez-Abadías et al., 2013; Meng et al., 2014; Sanderson et al., 2014). Interestingly, B6-Co eyelids were developmentally similar to that of wild-type B6 mice at E14.5. Therefore, it was difficult to distinguish between them at this stage (Figure 1A and B). However, at E16.5, the eyelids of B6-Co mice demonstrated significant retardation in development and did not close, compared to B6 mice (Figure 1C and D). After E16.5, eyelid

growth was slowed during development in B6-Co mice, and the eyelids remained open even at P0 (Figure 1E-H). It has been reported that the best time for eyelid closure is about E16.5, at which time the cornea and other eye accessory structures involved in gradual development could interfere with fusion of the upper and lower eyelids (McCauley et al., 2014; Heude et al., 2015). The eyelids of B6-Co mice grew slowly, and therefore missed the ideal period for eyelid fusion, demonstrating temporal and spatial specificity in embryonic development.

The developing eyelids are composed of loose mesenchyme covered by an epithelial sheet, the epidermis (outer surface), and conjunctiva (inner surface), as well as the periderm, which covers the epidermis (Deng et al., 2006). Only the peridermal and epidermal layers are involved in eyelid fusion. The mesenchymal layers of the upper and lower eyelids remain separate. A profusion of rounded periderm cells then appear, and pile up at the leading edges of the advancing eyelids during eyelid growth (Zhang et al., 2003b). Once contact is made between the opposed eyelids, these cells flatten and form a strip along the fusion line, until they slough off with the rest of the periderm on day 17 of gestation (Zhang et al., 2005). It is evident that the eyelids fused and reopened from the embryonic stage to about P14 to protect internal composition in the eye, especially the cornea. The eyelids were tightly closed at birth (Figure 1GIII). This was possibly the result of biological evolution, and we speculate that the eyeball was placed into physical homeostasis before the eyelids reopened. In contrast, eyelids opened at birth in B6-Co mice. The failure of this protection system in B6-Co mice leaves eyeballs exposed to an external environment, resulting in ocular diseases. The cornea gradually became opaque with neovessel formation observed (Figure 2BIII). This may be due to infectious materials in the housing cage and the environment. This phenotype was similar to that observed in Tg $\alpha$ -deficient mice (Pennock et al., 2011).

Development of corneal opacity was due to the environment or to a concurrent internal gene defect. Here, MEKK1-deficient mice were used to investigate the mechanism of corneal opacity formation. Several studies have shown that MEKK1 is required for B and T cell activation (Zhang et al., 2003a; Labuda et al., 2006; Kim et al., 2007). MEKK1 is necessary for CD40-mediated activation of Jnk and p38 kinases, and it is an essential component of signaling cascades involved in thymus-dependent antigen-induced B cell proliferation and antibody production (Gallagher et al., 2007). The MEKK1 kinase domain has been shown to be important for IL4 and IL6 gene expression under Th2 conditions (Enzler et al., 2009). Therefore, defects in immune function could account for corneal opacity, as well as the EOB phenotype in MEKK1-deficient mice. Further studies are needed to determine the effects of defects on the immune protective function, and the influence on defective corneal development.

Cell migration is required for upper and lower eyelid growth and development. Some EOB mice exhibit impaired cell migration in keratinocytes and fibroblasts cultured *in vitro*. Cell migration is also closely related to cell morphology, therefore the morphology of the cytoskeleton or microfilament bundles has been used to determine cell migration (Jin et al., 2008; Rice et al., 2012). MEKK1<sup>-/-</sup> cells have a flattened “pancake”-like morphology, whereas wild-type cells have a more spindle morphology, with a characteristic leading edge and tail (Yujiri et al., 1998). In the present study, the morphology of F-actin bundles and the nucleus exhibited a spindle shape in the leading edge of B6 mice, but a round shape in B6-Co mice (Figure 3). Laser-ablation experiments have shown that actin cables can generate a contractile force, which is responsible for movement of the epithelial sheet during dorsal closure, thereby functioning in a manner analogous to a purse string (Hutson et al., 2003). It is possible that the “string” is defective in B6-Co mice, and we propose that the structure or driving force led

to the defective “string”. This driving force was possibly impaired in *Rock1*<sup>-/-</sup> mice (Shimizu et al., 2005). Actin filaments were observed to be in an extended state in the leading edge of B6 mice (Figure 3AII). Therefore, we propose that the leading edge likely plays a “vanguard” role in the forward movement of the eyelids. The distinction in actin filament shape between B6 and B6-Co was evident at E16.5 and gradually decreased at E18.5 and P0 (Figure 3CII, DII, EII, and FII). The shape of the leading edge was blunt in B6-Co mice (Figure 3BII, arrowheads) but had a sharp tip in B6 mice (Figure 3AI), suggesting that migration direction of the leading edge was probably impaired in B6-Co mice. The development eyelids were divided into three fine structures, including root region (Figure 3(1) and (2), arrowheads), mesenchyme (Figure 3AII), and leading edge (Figure 3II, dotted line). Growth factors such as FGF10 from mesenchyme cells arrived at the leading edge and promoted their proliferation and migration (Tao et al., 2005). Keratinocyte migration was defective in B6-Co mice.

Cell proliferation and apoptosis were required for eyelid development and migration. A previous study showed that impaired cell proliferation was associated with eyelid closure (Mongan et al., 2011). Other studies also reported that apoptosis affects this process. According to our results, apoptosis and proliferation are not involved in eyelid fusion failure.

The process of eyelid development demonstrated temporal and spatial specificity in mice. Several necessary factors enhanced eyelid fusion in wild-type mice. In contrast, absence or shortage of these necessary factors was observed in the eyelids of gene-deficient mice. Furthermore, tissue specific of cornea was observed near the eyelids and no abundant alternative compensatory factors were identified. Therefore, the epithelium in eyelids moved very slowly. There was no significant difference in cell migration ability, as determined using a wound-healing assay, between adult wild-type and *MEKK1*<sup>-/-</sup> mice exhibiting the EOB phenotype (Deng et al., 2006). It is likely that abundant subcutaneous cytokines may serve as an alternative pathway to promote wound healing. A similar experiment was performed in *Rock1*<sup>-/-</sup> mice, *ROCK1* was not required for wound healing in adult skin, which further indicated that eyelid development was a process of temporal and spatial specificity in mice (Shimizu et al., 2005). Necessary factors for eyelid development can be applied to eyelid tissue *in vitro* in order to study the mechanism of action of these factors in eyelid development (Tao et al., 2005). Eyelid tissue culture *in vitro* vividly exhibits eyelid development, as well as temporal and spatial specificity, compared to keratinocytes cultured *in vitro*.

Mapping and identification of mutant genes are difficult using a phenotype driving method. B6-Co mice are a mutant strain induced by ENU administration. The mutant gene is located between 112,546,283 and 113,397,654 bp on chromosome 13 by SNPs (Jiang et al., 2010). Moreover, according to previous studies, *Map3k1* was the most likely mutated gene in B6-Co mice; however, no mutated sites were identified by sequencing (data not shown) (Warr et al., 2011). The mapping region possibly contains errors, because it is probably based on linkage disequilibrium in heredity. Therefore, we expanded the region to search for mutated genes; however, no mutations were observed in the *Plk2* gene (data not shown) but in the *Fgf10* (Figure 7A-E) and *Mtap1B* (Figure 7H) genes. The mutant sites of *Fgf10* and *Mtap1B* were not observed in all B6-Co samples (Table 2). However, the effect of these genes cannot be dismissed, because it is evident that the combined action of the environment and genes combine to generate the EOB phenotype. The regulation of multiple genes is possible in B6-Co mice, and further studies are needed to elucidate the genetic mechanism. Interestingly, there are no reports concerning genes related to the EOB phenotype in our mapping region, besides *Map3k1* and *Plk2*. Therefore, it is possible that there are some mutated sites in vast

noncoding regions or unknown functionally deficient genes in B6-Co mice.

Hbegf mRNA levels were significantly down-regulated at E16.5 in B6-Co eyelid tissues ( $P < 0.05$ ). However, the difference was not significant at E18.5 (Figure 8). We propose that various genes regulate different eyelid development stages. The B6-Co eyelid phenotype was similar to that observed in Hbegf-deficient mice, but abnormal eyelid development in both models is induced by different mechanisms.

Mouse embryonic eyelid closure, involving the movement of epithelial sheets, is a tissue morphogenetic process occurring in several physiological or pathological procedures. Many signaling pathways controlling eyelid closure might also be effective in epidermal wound healing and tumorigenesis, both requiring epithelial cell migration and morphogenesis. It is therefore not surprising that c-Jun-null mice showed reduced skin wound healing and tumor formation (Xia and Kao, 2004). Future studies should therefore explore the mechanism of action of important factors related to skin wound healing, as well as potential drug targets to treat impaired eyelid development. Ideally, eyelid closure should be achieved in mice exhibiting the EOB phenotype following treatment with various factors. There are few reports about eyelid function and eye accessory organs in adult EOB mice, because many studies have been focused on eyelid development at various embryonic stages. A previous study reported that shrinkage of the harderian gland in Fgf10 mutant mice could lead to corneal disease, due to defects in eyeball wetting (Puk et al., 2009). In conclusion, studies on eyelid function in EOB models would promote early diagnosis, prevention, and therapy for human heredity congenital eye disease, and development of relevant drugs. Furthermore, it could provide effective methods to understand and study human ocular diseases.

## Conflicts of interest

The authors declare no conflict of interest.

## ACKNOWLEDGMENTS

Research supported by the Natural Science Foundation of Jiangsu Province (#BK2010279), the Graduate Science and Technology Innovation Project of Nantong University (#YKC10015), and the Natural Science Foundation of the Higher Education Institutions of Jiangsu Province, China (#11KJB180010).

## REFERENCES

- Chucair-Elliott AJ, Elliott MH, Wang J, Moiseyev GP, et al. (2012). Leukemia inhibitory factor coordinates the down-regulation of the visual cycle in the retina and retinal-pigmented epithelium. *J. Biol. Chem.* 287: 24092-24102. <http://dx.doi.org/10.1074/jbc.M112.378240>
- Deng M, Chen WL, Takatori A, Peng Z, et al. (2006). A role for the mitogen-activated protein kinase kinase kinase 1 in epithelial wound healing. *Mol. Biol. Cell* 17: 3446-3455. <http://dx.doi.org/10.1091/mbc.E06-02-0102>
- Enzler T, Chang X, Facchinetti V, Melino G, et al. (2009). MEKK1 binds HECT E3 ligase Itch by its amino-terminal RING motif to regulate Th2 cytokine gene expression. *J. Immunol.* 183: 3831-3838. <http://dx.doi.org/10.4049/jimmunol.0803412>
- Gallagher E, Enzler T, Matsuzawa A, Anzelon-Mills A, et al. (2007). Kinase MEKK1 is required for CD40-dependent activation of the kinases Jnk and p38, germinal center formation, B cell proliferation and antibody production. *Nat. Immunol.* 8: 57-63. <http://dx.doi.org/10.1038/ni1421>
- Harris MJ and Juriloff DM (1986). Eyelid development and fusion induced by cortisone treatment in mutant, lidgap-Miller, foetal mice. A scanning electron microscope study. *J. Embryol. Exp. Morphol.* 91: 1-18.

- Hayashi Y, Liu CY, Jester JJ, Hayashi M, et al. (2005). Excess biglycan causes eyelid malformation by perturbing muscle development and TGF- $\alpha$  signaling. *Dev. Biol.* 277: 222-234. <http://dx.doi.org/10.1016/j.ydbio.2004.09.022>
- Heude É, Bellessort B, Fontaine A, Hamazaki M, et al. (2015). Etiology of craniofacial malformations in mouse models of blepharophimosis, ptosis and epicanthus inversus syndrome. *Hum. Mol. Genet.* 24: 1670-1681. <http://dx.doi.org/10.1093/hmg/ddu579>
- Hutson MS, Tokutake Y, Chang MS, Bloor JW, et al. (2003). Forces for morphogenesis investigated with laser microsurgery and quantitative modeling. *Science* 300: 145-149. <http://dx.doi.org/10.1126/science.1079552>
- Jiang YM, Liu C, Wu LC and Shao YX (2010). Fine mapping of mutant gene related corneal opacity mouse with SNPs. *Yi chuan = Hereditas/ Zhongguo yi chuan xue hui bian ji.* 32: 486-491. [Article in Chinese].
- Jin C, Yin F, Lin M, Li H, et al. (2008). GPR48 regulates epithelial cell proliferation and migration by activating EGFR during eyelid development. *Invest. Ophthalmol. Vis. Sci.* 49: 4245-4253. <http://dx.doi.org/10.1167/iovs.08-1860>
- Juriloff DM, Harris MJ and Mah DG (2005). The open-eyelid mutation, lidgap-Gates, is an eight-exon deletion in the mouse Map3k1 gene. *Genomics* 85: 139-142. <http://dx.doi.org/10.1016/j.ygeno.2004.10.002>
- Kato S, Mohri Y, Matsuo T, Ogawa E, et al. (2007). Eye-open at birth phenotype with reduced keratinocyte motility in LGR4 null mice. *FEBS Lett.* 581: 4685-4690. <http://dx.doi.org/10.1016/j.febslet.2007.08.064>
- Kim MJ, Chae JS, Kim KJ, Hwang SG, et al. (2007). Negative regulation of SEK1 signaling by serum- and glucocorticoid-inducible protein kinase 1. *EMBO J.* 26: 3075-3085. <http://dx.doi.org/10.1038/sj.emboj.7601755>
- Labuda T, Christensen JP, Rasmussen S, Bonnesen B, et al. (2006). MEK kinase 1 is a negative regulator of virus-specific CD8(+) T cells. *Eur. J. Immunol.* 36: 2076-2084. <http://dx.doi.org/10.1002/eji.200535163>
- Li G, Gustafson-Brown C, Hanks SK, Nason K, et al. (2003). c-Jun is essential for organization of the epidermal leading edge. *Dev. Cell* 4: 865-877. [http://dx.doi.org/10.1016/S1534-5807\(03\)00159-X](http://dx.doi.org/10.1016/S1534-5807(03)00159-X)
- Lin WC, Wang LC, Pang TL and Chen MY (2015). Actin-binding protein G (AbpG) participates in modulating the actin cytoskeleton and cell migration in *Dictyostelium discoideum*. *Mol. Biol. Cell* 26: 1084-1097. <http://dx.doi.org/10.1091/mbc.E14-05-0972>
- Ma S, Charron J and Erikson RL (2003). Role of Plk2 (Snk) in mouse development and cell proliferation. *Mol. Cell. Biol.* 23: 6936-6943. <http://dx.doi.org/10.1128/MCB.23.19.6936-6943.2003>
- Martínez-Abadías N, Motch SM, Pankratz TL, Wang Y, et al. (2013). Tissue-specific responses to aberrant FGF signaling in complex head phenotypes. *Dev. Dyn.* 242: 80-94. <http://dx.doi.org/10.1002/dvdy.23903>
- McCaughey HA, Liu CY, Attia AC, Wikenheiser-Brokamp KA, et al. (2014). TGF $\beta$  signaling inhibits goblet cell differentiation via SPDEF in conjunctival epithelium. *Development* 141: 4628-4639. <http://dx.doi.org/10.1242/dev.117804>
- Meixner A, Haverkamp S, Wässle H, Führer S, et al. (2000). MAP1B is required for axon guidance and is involved in the development of the central and peripheral nervous system. *J. Cell Biol.* 151: 1169-1178. <http://dx.doi.org/10.1083/jcb.151.6.1169>
- Meng Q, Mongan M, Carreira V, Kurita H, et al. (2014). Eyelid closure in embryogenesis is required for ocular adnexa development. *Invest. Ophthalmol. Vis. Sci.* 55: 7652-7661. <http://dx.doi.org/10.1167/iovs.14-15155>
- Mine N, Iwamoto R and Mekada E (2005). HB-EGF promotes epithelial cell migration in eyelid development. *Development* 132: 4317-4326. <http://dx.doi.org/10.1242/dev.02030>
- Mongan M, Wang J, Liu H, Fan Y, et al. (2011). Loss of MAP3K1 enhances proliferation and apoptosis during retinal development. *Development* 138: 4001-4012. <http://dx.doi.org/10.1242/dev.065003>
- Pacal M and Bremner R (2014). Induction of the ganglion cell differentiation program in human retinal progenitors before cell cycle exit. *Dev. Dyn.* 243: 712-729. <http://dx.doi.org/10.1002/dvdy.24103>
- Pennock S, Rheume MA, Mukai S and Kazlauskas A (2011). A novel strategy to develop therapeutic approaches to prevent proliferative vitreoretinopathy. *Am. J. Pathol.* 179: 2931-2940. <http://dx.doi.org/10.1016/j.ajpath.2011.08.043>
- Puk O, Esposito I, Söker T, Löster J, et al. (2009). A new Fgf10 mutation in the mouse leads to atrophy of the Harderian gland and slit-eye phenotype in heterozygotes: a novel model for dry-eye disease? *Invest. Ophthalmol. Vis. Sci.* 50: 4311-4318. <http://dx.doi.org/10.1167/iovs.09-3451>
- Ricardo NS and Miller JR (1967). Further observations on lg MI (lid-gap Miller) and other open-eye mutants in the house mouse. *Can. J. Genet. Cytol.* 9: 596-605. <http://dx.doi.org/10.1139/g67-064>
- Rice DS, Hansen GM, Liu F, Crist MJ, et al. (2012). Keratinocyte migration in the developing eyelid requires LIMK2. *PLoS One* 7: e47168. <http://dx.doi.org/10.1371/journal.pone.0047168>
- Sanderson J, Dartt DA, Trinkaus-Randall V, Pintor J, et al. (2014). Purines in the eye: recent evidence for the physiological and pathological role of purines in the RPE, retinal neurons, astrocytes, Müller cells, lens, trabecular meshwork, cornea and lacrimal gland. *Exp. Eye Res.* 127: 270-279. <http://dx.doi.org/10.1016/j.exer.2014.08.009>
- Shao Y, Wu B, Xue Z, Chen B, et al. (2006). The New Mutation Mouse with Heritable Disease of Cornea Matrix Denaturalization and the Mapping of Mutation Gene. *Chin. J. J. Nanjing Normal Univ. (Natural Science)* 29: 99-102. [Article in Chinese].

- Shimizu Y, Thumkeo D, Keel J, Ishizaki T, et al. (2005). ROCK-I regulates closure of the eyelids and ventral body wall by inducing assembly of actomyosin bundles. *J. Cell Biol.* 168: 941-953. <http://dx.doi.org/10.1083/jcb.200411179>
- Tang JZ, Zhu CL, Shao YX, Guan HJ, et al. (2008). Observation of ultramicro-pathology in the keratitis model of mouse with genetic deficiency. *Chin. J. Clin. Exp. Pathol.* 24: 593-595.
- Tao H, Shimizu M, Kusumoto R, Ono K, et al. (2005). A dual role of FGF10 in proliferation and coordinated migration of epithelial leading edge cells during mouse eyelid development. *Development* 132: 3217-3230. <http://dx.doi.org/10.1242/dev.01892>
- Thumkeo D, Shimizu Y, Sakamoto S, Yamada S, et al. (2005). ROCK-I and ROCK-II cooperatively regulate closure of eyelid and ventral body wall in mouse embryo. *Genes Cells* 10: 825-834. <http://dx.doi.org/10.1111/j.1365-2443.2005.00882.x>
- Tsau C, Ito M, Gromova A, Hoffman MP, et al. (2011). Barx2 and Fgf10 regulate ocular glands branching morphogenesis by controlling extracellular matrix remodeling. *Development* 138: 3307-3317. <http://dx.doi.org/10.1242/dev.066241>
- Warr N, Bogani D, Siggers P, Brixey R, et al. (2011). Minor abnormalities of testis development in mice lacking the gene encoding the MAPK signalling component, MAP3K1. *PLoS One* 6: e19572. <http://dx.doi.org/10.1371/journal.pone.0019572>
- Xia Y and Kao WW (2004). The signaling pathways in tissue morphogenesis: a lesson from mice with eye-open at birth phenotype. *Biochem. Pharmacol.* 68: 997-1001. <http://dx.doi.org/10.1016/j.bcp.2004.05.028>
- Yujiri T, Sather S, Fanger GR and Johnson GL (1998). Role of MEKK1 in cell survival and activation of JNK and ERK pathways defined by targeted gene disruption. *Science* 282: 1911-1914. <http://dx.doi.org/10.1126/science.282.5395.1911>
- Zhang L, Deng M, Kao CW, Kao WW, et al. (2003a). MEK kinase 1 regulates c-Jun phosphorylation in the control of corneal morphogenesis. *Mol. Vis.* 9: 584-593.
- Zhang L, Wang W, Hayashi Y, Jester JV, et al. (2003b). A role for MEK kinase 1 in TGF-beta/activin-induced epithelium movement and embryonic eyelid closure. *EMBO J.* 22: 4443-4454. <http://dx.doi.org/10.1093/emboj/cdg440>